# *K*-shell and *L*-shell $(e,3e)$ double ionization of beryllium by fast electron impact

M. Becher* and B. Joulakian†
*Laboratoire de Physique Moléculaire et des Collisions, membre FR CNRS 2843 Jean Barriol, Université Paul Verlaine–Metz, 1 Boulevard Arago, 57078 Metz Cedex 3, France*

C. Le Sech‡
*Laboratoire des Collisions Atomiques et Moléculaires, UMR CNRS 8625, Université Paris XI, Bâtiment 351, F-91405 Orsay Cedex, France*

M. Chrysos§
*Laboratoire des Propriétés Optiques des Matériaux et Applications, UMR CNRS 6136, Université d'Angers, 2 Boulevard Lavoisier, 49045 Angers Cedex, France*

(Received 9 November 2007; published 19 May 2008)

We report fully differential cross sections for simultaneous double ionization of atomic beryllium by fast electron impact. We analyze separately the two ionization channels that leave the dication in either the $2s^2$ autoionizing excited state or its $1s^2$ bound ground state. For the double continuum, owing to the two slow emitted electrons, we employ the three-pairwise-Coulomb-interaction model (3C) along with the first Born approximation. Aiming to probe the hitherto largely unexplored role of the electron correlation in $(e,3e)$, we determine and check fully correlated, compact analytical wave functions, satisfying all two-particle Kato cusp conditions for the four-electron Be initial state and the two-electron $Be^{2+}$ final states, as well as other, much or little or noncorrelated, functions, issuing from either analytic global optimization or Hartree-Fock theory. We point out similarities or contrasts with trends observed in the double photoionization, allowing for parallels between $(e,3e)$ and $(\gamma,2e)$. Various numerical examples serve to navigate possible future experiments in the nonrelativistic regime of the ionization problem.

DOI: 10.1103/PhysRevA.77.052710 PACS number(s): 34.80.Dp

## I. INTRODUCTION

The so-called $(e,3e)$ process has been for several decades a hot topic of atomic and molecular collision theory at the interface between fundamental and applied physics. Technically, this process consists in simultaneously detecting, with a coincidence experiment, the electrons emerging in the electron-impact double ionization of atoms or molecules. There are several good reasons why studies of the $(e,3e)$ process have been attracting much attention in recent years. The experimental and theoretical results associated with the process propose themselves as key elements for answering open questions about the *N*-body problem with Coulomb interactions and strongly correlated initial and final states. Furthermore, as the $(e,3e)$ differential cross sections are often sensitive to the preparation of the target, analysis of the collision dynamics can be a powerful tool for understanding structural details of doubly excited states. On the other hand, it is believed that the $(e,3e)$ process can be an invaluable device for plasma diagnostics, biophysics, and astrophysics, as being particularly effective for transferring appreciable amounts of energy and storing it in the target.

A great deal of work has been devoted so far to the double ionization of light atoms, and especially of their prototype, helium. Byron and Joachain [1], Tweed [2,3], Neudatchin *et al.* [4], and Smirnov *et al.* [5] have been recognized for pioneering contributions to the subject. Later, theoretical support was provided by Dal Cappello and Le Rouzo [6] and by Joulakian *et al.* [7,8] to the first experiments carried out by Lahman-Bennani *et al.* [9,10] and Ford *et al.* [11]. In recent years, experimental efforts [12–15] are being concentrated on improving the energy resolution for the determination of the multiply differential cross section of the $(e,3e)$ process, and there is also emphasis on developing accurate theoretical approaches for thorough study of double photoionization [16], ion-impact double ionization [17], fast charged-particle-impact double ionization [18–20], and electron-impact double ionization [21–24].

Beryllium vapor has recently become a subject of growing attention for fundamental research, because of its role in inelastic scattering. This too is the case with beryllium plasma for applied research. This is because of the shielding layer on graphite that such a plasma creates, which may be of usefulness in studying erosion effects in the International Thermonuclear Experimental Reactor fusion device [25]. Most significant has been the progress over the last five years. Wang *et al.* [26], Zhang *et al.* [27], and Wang *et al.* [28] explored the beryllium full electronic structure by including relativistic effects in the total Hamiltonian. In the field of inelastic collisions, Hasegawa and co-workers [29,30] studied the photo-double-excitation of hollow beryllium, for both the *L* and *K* shells, and did Dirac-Fock calculations to identify or predict hollow resonance peaks. Kheifets and Bray [31,32] employed the convergent close-

*becher@univ-metz.fr
†joulak@sciences.univ-metz.fr
‡lesech@lcam.u-psud.fr
§michel.chrysos@univ-angers.fr

 

coupling (CCC) approach to study the photo-double- and photo-triple-ionization of the atom, within the frozen-core approximation and the double shake-off model, respectively. Colgan *et al.* [33] developed a time-dependent close-coupling approach to monitor, over time, the electron-beryllium ionization process. Finally, in a recent mathematical treatment of the *L*-shell photo-double-ionization of berylliumlike ions, Nefiodov and Plunien [34] established the double-to-single ionization cross section ratio and explained how the double photoionization cross section is shared between simultaneous and sequential channels.

The scope of this paper is twofold. Primarily, it aims at reporting on the beryllium fully differential *K*- and *L*-shell double ionization cross sections by fast electron impact. The study focuses on the $(e,3e)$ process, which (by definition) refers to the simultaneous ionization of two atomic electrons,

$$e^- + \mathrm{Be} \rightarrow 3e^- + \mathrm{Be}^{2+}.$$

Even though the simultaneous double ionization of the Be *L*-shell electrons competes with a sequential process taking place via a nonradiative electron emission of the transiently formed $1s2s^2$ resonance state of $\mathrm{Be}^{+*}$,

$$e^- + \mathrm{Be} \rightarrow 2e^- + \mathrm{Be}^{+*} \underset{\text{resonance}}{\rightarrow} 3e^- + \mathrm{Be}^{2+},$$

time-of-flight coincidence experiments allow one nowadays to distinguish between the two channels. This is a prerequisite when conducting a double ionization experiment in beryllium, especially in light of recent findings showing the sequential process to be by far the dominant channel [34]. In order to accomplish the task, smart analytical wave functions satisfying cusp conditions are developed and employed, as a compromise between accuracy and numerical economy. Then, we proceed to comparison of the most striking cross section features issuing from the different calculations, to probe the relative impact of the electron correlation, which for fast collision processes is thought to be the main cause of the double ionization. Throughout the analysis, some analogies are found between $(e,3e)$ and $(\gamma,2e)$ processes, as to trends common or opposite in the two processes. It is worth pointing out that, according to whether it is the *L*- or the *K*-shell electrons that are doubly ionized, distinct final states must be considered: the $\mathrm{Be}^{2+}$ ground state $1s^2$ in the former case, and the doubly excited $2s^2$ autoionizing state of the dication in the latter case. Note that, experimentally, the total energy conservation principle makes it possible to distinguish between the two channels, since the difference between the two ionization potential values by far exceeds the energy resolution limit in a typical experimental setup ($\approx$4 eV). Atomic units (a.u.) are used throughout, unless otherwise stated.

## II. THEORY

### A. Structure, symmetry, and transition amplitude

The quantitative understanding of the collision between a fast electron (the projectile) and Be (the target) requires an exhaustive analysis of the four-electron atomic target as well as the construction of sufficiently accurate wave functions for initial and final states of a "five-electron composite system." Although the compact electron core of Be is well separated, both in the coordinate space and in energy, from the valence $ns^2$ shell [31], here, the four-electron problem is addressed from first principles, which makes the use of model potentials [35] for core effects redundant. The motivation for such a treatment stems from the need for a rigorous consideration of the process, especially in the case of ionization of the core, in which the treatment of the inner electrons as simple "spectators" can no longer be justified.

Initially, Be is supposed to be in its ground state, which is spinless. The value of the total spin magnetic quantum number $M_S$ of the composite system is thus imposed by the spin of the incident electron. Although wave functions going beyond the single-electron orbital concept turn out to be more effective for our purposes (see below), in this section the structure of the Be ground state is discussed as an admixture $c_{1s^2 2s^2} 1s^2 2s^2 + c_{1s^2 2p^2} 1s^2 2p^2$ ($^1S$) within the conventional orbital description, so that the general aspects of the treatment are outlined pedagogically. In doing this, the initial-state wave function for $M_S = \frac{1}{2}$ is expressed as a symmetry-adapted combination of Slater determinants, constructed by products between the incident wave $\chi_i$ and the atomic spin orbitals $\varphi_{nlm_l}$ and $\bar{\varphi}_{nlm_l}$ ($n,l,m_l$ stand for the principal, orbital, and orbital magnetic quantum numbers) for spin-up and spin-down monoelectronic $1s$, $2s$, or $2p$ states, respectively:

$$\begin{aligned}\Psi_{i\uparrow} = {} & c_{1s^2 2s^2} |\chi_i \varphi_{100} \bar{\varphi}_{100} \varphi_{200} \bar{\varphi}_{200}| \rangle \\ & + c_{1s^2 2p^2} \frac{1}{\sqrt{3}} (|\chi_i \varphi_{100} \bar{\varphi}_{100} \varphi_{211} \bar{\varphi}_{21-1}| \rangle \\ & - |\chi_i \varphi_{100} \bar{\varphi}_{100} \varphi_{210} \bar{\varphi}_{210}| \rangle + |\chi_i \varphi_{100} \bar{\varphi}_{100} \varphi_{21-1} \bar{\varphi}_{211}| \rangle).\end{aligned} \tag{1}$$

In the above equation, $|a_1 a_2 \cdots a_N|$ are normalized Slater determinants; the indices $i$ and $\uparrow$ in $\Psi_{i\uparrow}$ denote the initial and spin-up states, respectively, and the index $i$ in $\chi_i$ denotes incident; the quantities $c_{1s^2 2s^2}$ and $c_{1s^2 2p^2}$ are mixing coefficients.

In the final state, three free and two bound electrons are involved: the scattered electron, with a wave function $\chi_s$, the two ejected electrons, with wave functions $\chi_1$ and $\chi_2$, and the two electrons of the residual ion. For the sake of simplicity of presentation, the state of the ion is here represented by spin orbitals $\phi_{nlm_l}$ and $\bar{\phi}_{nlm_l}$, within either a single-configuration ($1s^2$) or a two-configuration ($c_{2s^2} 2s^2 + c_{2p^2} 2p^2$) description, in a way analogous to the above. In this respect, the wave function of the final state for $M_S = \frac{1}{2}$ is $\Psi_{f\uparrow} = \frac{1}{\sqrt{2}} |D_1 - D_2\rangle$, where the index $f$ in $\Psi_{f\uparrow}$ denotes final, and $D_1$ and $D_2$ are single Slater determinants or appropriate combinations of Slater determinants according to whether it is the $1s^2$ or the $c_{2s^2} 2s^2 + c_{2p^2} 2p^2$ state that is concerned.

In the first Born approximation, which should be adequate at high impact energies, the total spin is conserved because the spin operator is absent from the perturbation potential (see below). The double ionization fully differential cross section (FDCS), which is fivefold, reads

$$\sigma^{(5)} = \frac{d^5\sigma}{d\theta_s d\Omega_1 d\Omega_2 dE_1 dE_2} = (2\pi)^4 \frac{k_1 k_2 k_s}{k_i} |T_{fi}|^2 \qquad (2)$$

with $k_i$, $k_s$, $k_1$, and $k_2$ the asymptotic momenta of the incident, scattered, and two ejected electrons, respectively, $E_1$, $E_2$, $\Omega_1$, and $\Omega_2$ the energies and the solid angles of the ejected electrons, and $\theta_s$ the polar scattering angle with respect to the direction of the incident electron. $T_{fi}=\frac{1}{\sqrt{2}}\langle D_1 - D_2|V|\Psi_{i\uparrow}\rangle$ designates the $f \leftarrow i$ transition matrix element $\langle\Psi_f|V|\Psi_i\rangle$ of the perturbation $V$ given by the first term of the Born series. In the above, we have tacitly admitted that half of the incident electrons in the beam are upwardly polarized and the other half are downwardly polarized. The operator $V$ is the interaction potential $V=-\frac{Z}{r_0}+\Sigma_{j=1}^{Z}\frac{1}{|\vec{r}_0-\vec{r}_j|}$ experienced by the incident electron, with $Z=4$; $\vec{r}_0$ is the position vector of the incident electron with respect to the nucleus, the latter being taken as the origin $(O)$; $\vec{r}_j$ is the position vector of the target's $j$th electron $(j=1-4)$ with respect to $O$.

The development of Eq. (2) involves as many as 18 different exchange integrals. Here, however, we address fast projectiles (>1 keV) and (relatively) slow ejected electrons, and only two integrals can survive in practice among the possible combinations that are formally present. $T_{fi}$ reads

$$T_{fi} \approx \sqrt{2}(f_1 + f_2) \qquad (3)$$

with

$$f_1 = \langle\chi_s(\vec{k}_s,\vec{r}_0)\psi(\vec{r}_1,\vec{r}_2)\xi(\vec{k}_1,\vec{r}_3;\vec{k}_2,\vec{r}_4)|V|\chi_i(\vec{k}_i,\vec{r}_0)\Phi(\vec{r}_1,\vec{r}_2,\vec{r}_3,\vec{r}_4)\rangle,$$

$$f_2 = \langle\chi_s(\vec{k}_s,\vec{r}_0)\psi(\vec{r}_3,\vec{r}_4)\xi(\vec{k}_1,\vec{r}_1;\vec{k}_2,\vec{r}_2)|V|\chi_i(\vec{k}_i,\vec{r}_0)\Phi(\vec{r}_1,\vec{r}_2,\vec{r}_3,\vec{r}_4)\rangle. \qquad (4)$$

In these expressions, $\xi$ represents the double continuum of the two ejected electrons; its explicit form is given in the next section. $\Phi(\vec{r}_1,\vec{r}_2,\vec{r}_3,\vec{r}_4)$ denotes the four-electron target wave function. Finally, $\psi$ stands for the normalized two-electron bound state wave function of the residual dication. Rigorously, in the case of the *K*-shell ionization, $\psi$ is an autoionizing state with a finite lifetime rather than a truly bound state whose lifetime would be infinite. Such states are embedded in the continuum, for they lie above the first ionization threshold of $Be^{3+}$. Their instability manifests itself by a spontaneous relaxation of the bielectronic system into a free electron and a residual bound hydrogenlike trication [36]. However, in the present case, these are final states, and as such, their finite lifetime has absolutely no effect on the course of the $(e,3e)$ process. Note that, in Eq. (4), the scattered electron has been supplied with the same position vector $\vec{r}_0$ as the incident one. Whether the electron is incident or scattered depends only on whether it is the initial state or the final state that is addressed. Unlike $\vec{r}_0$, which varies continuously during the process, the wave vector $\vec{k}_i$ switches upon impact to $\vec{k}_s$. For a neutral target, both the fast incident electron $i$ and the scattered one $s$ can be represented by plane waves. This simplification allows the use, in Eq. (4), of the Bethe integral over the space coordinate $\vec{r}_0$, and results in

$$f_1 = \frac{1}{2\pi^2 K^2}\langle\psi(\vec{r}_1,\vec{r}_2)\xi(\vec{k}_1,\vec{r}_3;\vec{k}_2,\vec{r}_4)|U|\Phi(\vec{r}_1,\vec{r}_2,\vec{r}_3,\vec{r}_4)\rangle. \qquad (5)$$

A similar expression is obtained for $f_2$, in a way analogous to the way in which $f_2$ is defined from Eq. (4). Here, $U$ designates the effective potential $U=-Z+\Sigma_{i=1}^{4}e^{i\vec{K}\cdot\vec{r}_i}$, and $\vec{K}=\vec{k}_i-\vec{k}_s$ is the momentum transfer vector, that is, the amount of momentum that is transferred by the projectile into the target.

### B. The wave functions

In order to determine the transition amplitude $T_{fi}$, we need properly optimized wave functions for the four-electron target and the residual two-electron ion. The wave functions of the small Coulombic systems involved in inelastic collisions must be accurate enough to allow good understanding of the phenomena that govern the electron dynamics. At the same time, they must be compact enough to allow the economic treatment of the problem, whose computational difficulty is generally great. In contrast with numerical or analytic wave functions involving configuration interaction (CI) optimization, or self-consistent field (SCF) procedures, or multiparameter Hylleraas-correlation functions, Jastrow wave functions [39,40] are very advantageous for they are surprisingly accurate, simple, and analytic.

#### *1. Initial state*

The initial state involves the $1s^2 2s^2\ ^1S$ ground state of Be. Its wave function, represented by $\Phi$ in Eq. (4), is expressed by a fully correlated Jastrow function of the form [41]

$$\Phi(\vec{r}_1,\vec{r}_2,\vec{r}_3,\vec{r}_4) = \frac{1}{\sqrt{N}}(\zeta_1 + a_{\mathrm{mix}}\zeta_2)J. \qquad (6)$$

This form is a generalization of a particular type of wave function originally proposed for two-electron systems [42]. In Eq. (6), $\zeta_1$, $\zeta_2$, and $J$ are defined by

$$\zeta_1 = R_{1s}(r_1)R_{1s}(r_2)R_{2s}(r_3)R_{2s}(r_4),$$

$$\zeta_2 = R_{1s}(r_1)R_{1s}(r_2)R_{2p}(r_3)R_{2p}(r_4)\cos\theta_{34}, \qquad (7)$$

in order to account for the $2s^2,2p^2\ ^1S$ degeneracy, and

$$J = \cosh(\lambda r_1)\cosh(\lambda r_2)\cosh(\lambda r_3)\cosh(\lambda r_4) \times \exp\left(\frac{r_{12}}{2(1+br_{12})}\right)\exp\left(\frac{r_{34}}{2(1+br_{34})}\right) \qquad (8)$$

with $R_{1s}$, $R_{2s}$, and $R_{2p}$, the unnormalized hydrogenic radial wave functions

$$R_{1s}(r) = e^{-Zr},$$

$$R_{2s}(r) = \left(1-\frac{Zr}{2}\right)e^{-Zr/2},$$

$$R_{2p}(r) = re^{-Zr/2}, \qquad (9)$$

$\cos\theta_{34}=\frac{r_3^2+r_4^2-r_{34}^2}{2r_3r_4}$, and $r_{ij}=|\vec{r}_i-\vec{r}_j|$ $(i,j=1,2,3,4)$. While $\Phi$ has not been given in the symmetrized form that is appropri-

ate for a many-electron wave function, all contributions to $T_{fi}$ owing to the missing permutational terms have been properly accounted for through Eqs. (3) and (4). For the specific problem at hand, the remaining four parameters appearing in Eqs. (6)–(9) take values $N=8.3277\times10^{-2}$, $a_{\mathrm{mix}}=-0.900$, $\lambda=0.88$, and $b=1.4$. An energy value of $-14.659$ a.u. was obtained, differing by only 0.05% from the "exact" nonrelativistic result, $E=-14.667$ a.u. [43], and containing 92.5% of the correlation energy with respect to the Hartree-Fock (HF) level, $E_{\mathrm{HF}}=-14.573$ a.u. [44].

It is worth pointing out that $\Phi$ satisfies all the required two-electron Kato cusp conditions. This is smartly ensured through the $\cosh(\lambda r_i)$ functions, which drop all terms linear in $r_i$ in the series development of the nonhydrogenic part of $\Phi$, and through the $\exp(\frac{r_{ij}}{2(1+br_{ij})})$ functions, which restore the correct $\frac{1}{2}$ slope of all terms linear in $r_{ij}$ in the corresponding series development. Wave functions satisfying cusp conditions are generally superior to those which do not, for they substantially improve accuracy without additional computational effort. Once their functional form has been properly chosen and free parameters optimized, such functions usually account for an overwhelming amount of electronic correlation. Among wave functions satisfying cusp conditions, the function of Eq. (6) is a very good representation of the Be ground state. Cross sections reported henceforward are calculated with this wave function for the initial state.

In order to assess the relative importance of correlation for double ionization, a less correlated variant of the Jastrow functions was also checked, obtained by neutralizing the explicit appearance of any interelectronic distance, i.e., $b\to\infty$. In doing this, $N=5.1599\times10^{-2}$, $a_{\mathrm{mix}}=-0.997$, and $\lambda=0.92$. An energy amounting to $E=-14.625$ a.u. was obtained, containing 56% of the correlation energy. Finally, the uncorrelated Clementi wave function, constructed with orbitals from the Clementi-Roetti data tables for the Be ground state on the basis of $1s^22s^2$ alone, and producing $E=-14.573$ a.u., was also used for comparison [45].

### 2. Final state

*a. The ejected electrons*. The final state involves two slow ejected electrons. These electrons bring into play a double continuum whose treatment requires use of a three-pairwise-Coulomb-interaction (3C) wave function. This representation for the double continuum was initially applied by Brauner, Briggs, and Klar [46] to the $(e,3e)$ ionization of hydrogen, and later by Joulakian, Dal Cappello, and Brauner [7], and by Joulakian and Dal Cappello [8], to the $(e,3e)$ ionization of helium. The 3C wave function is constructed as a suitable Coulomb-wave product $\xi$, involving three two-body Coulomb interactions. This product accounts approximately for the electron-electron correlation and satisfies, in most physical situations, the exact asymptotic boundary conditions. Symbolically,

$$\xi(\vec{k}_1,\vec{r}_1;\vec{k}_2,\vec{r}_2)=Me^{i\vec{k}_1\cdot\vec{r}_1}e^{i\vec{k}_2\cdot\vec{r}_2}\tilde{\chi}(\vec{r}_1,\vec{r}_2) \tag{10}$$

with

$$\tilde{\chi}(\vec{r}_1,\vec{r}_2)=\prod_{j=1}^{2}{}_1F_1(i\alpha_j,1;-i(k_jr_j+\vec{k}_j\cdot\vec{r}_j))\ {}_1F_1(i\alpha_{12},1;-i(k_{12}r_{12}+\vec{k}_{12}\cdot\vec{r}_{12})) \tag{11}$$

a function taking into account the repulsion between the two ejected electrons, and

$$M=\frac{1}{(2\pi)^3}e^{-\pi/2(\alpha_1+\alpha_2+\alpha_{12})}\Gamma(1-i\alpha_1)\Gamma(1-i\alpha_2)\Gamma(1-i\alpha_{12}). \tag{12}$$

In the above expressions, ${}_1F_1$ denotes the confluent hypergeometric series, $\Gamma$ is the Gamma function, $\vec{k}_{12}=(\vec{k}_1-\vec{k}_2)/2$, $\alpha_1=-Z/|\vec{k}_1|$, $\alpha_2=-Z/|\vec{k}_2|$, and $\alpha_{12}=1/|\vec{k}_1-\vec{k}_2|$. As pointed out above, $\tilde{\chi}$ is a simple product rather than a symmetrized one. The equally contributing missing term has already been accounted for in $T_{fi}$ through Eqs. (3) and (4).

*b. The residual ion*. The state of the dication is described by correlated wave functions for the ground state ($L$-shell ionization) and the doubly excited state ($K$-shell ionization). As before, Jastrow functions satisfying Kato's cusp conditions are used as a reference. In addition to these functions, a simple biparametric wave function is also discussed, whose parameters were globally optimized to the energy absolute minimum [47]. Finally, an uncorrelated analytic HF wave function ($E_{\mathrm{HF}}=-13.611$ a.u.) and a little correlated "HF" $s+p$ Slater-type orbital (STO) expansion ($E=-3.477$ a.u.) were used for the $1s^2$ and $2s^2$ states, respectively, and checked for comparison.

*Jastrow wave functions*. For the $2s^2$ state, the wave function is given the form

$$\psi(\vec{r}_1,\vec{r}_2)=\frac{1}{\sqrt{N}}e^{-Zr_1/2}e^{-Zr_2/2}\left[\left(1-\frac{Zr_1}{2}\right)\left(1-\frac{Zr_2}{2}\right)+a_{\mathrm{mix}}(r_1^2+r_2^2-r_{12}^2)\right][\cosh(\lambda r_1)+\cosh(\lambda r_2)]\exp\left(\frac{r_{12}}{2(1+br_{12})}\right). \tag{13}$$

This expression accounts for the heavy mixing between the two $ll$ subshells within the $n_1=n_2=2$ manifold. The extreme importance of the intrashell correlation in doubly excited states has been extensively stressed in the past, especially for ${}^1S^e$ states for which the equality between the orbital angular momenta of the two electrons is a prerequisite (for a review, see [48]). As before, this expression again satisfies, by virtue of $\cosh(\lambda r_1)$, $\cosh(\lambda r_2)$, and $\exp(\frac{r_{12}}{2(1+br_{12})})$, the three cusp conditions relevant to $r_1$, $r_2$, and $r_{12}$, respectively. The parameters of Eqs. (13) amount to $N=3.3395$, $a_{\mathrm{mix}}=-0.7043$, $\lambda=0.16$, and $b=0.35$. An energy value of $E=-3.542$ a.u. was found, which coincides with the exact nonrelativistic value to three significant figures.

For the ground $1s^2$ state of $Be^{2+}$, the wave function is given the form

$$\psi(\vec{r}_1,\vec{r}_2) = \frac{1}{\sqrt{N}} e^{-Zr_1} e^{-Zr_2} [\cosh(\lambda r_1) + \cosh(\lambda r_2)] \exp\left(\frac{r_{12}}{2(1+br_{12})}\right), \tag{14}$$

in agreement with the three Kato requirements. For the specific problem at hand, the parameters appearing in Eqs. (14) were found to take values $N=1.6876\times10^{-2}$, $\lambda=0.91$, and $b=0.7$. An energy value of $E=-13.6518$ a.u., differing by only 0.028% from the "exact" nonrelativistic result $E=-13.6556$ [49] and containing 92% of the correlation energy, was obtained.

*Analytic global optimization*. As stressed above, the two-intrashell configuration interaction

$$\psi(\vec{r}_1,\vec{r}_2) = c_{2s^2}\psi_{2s^2} + c_{2p^2}\psi_{2p^2} \tag{15}$$

is the minimal requirement for the realistic representation of the doubly excited $2s^2$ state. Here, the $\psi_{2s^2}$ and $\psi_{2p^2}$ wave function components read

$$\psi_{2s^2} = \frac{1}{4\pi} R_{2,0}(r_1) R_{2,0}(r_2), \tag{16}$$

$$\psi_{2p^2} = -\frac{\sqrt{3}}{4\pi} R_{2,1}(r_1) R_{2,1}(r_2) \cos\theta, \tag{17}$$

with

$$R_{2,0}(r) = C(1-cr)e^{-\gamma r}, \quad R_{2,1}(r) = Dre^{-\delta r} \tag{18}$$

and $\theta \equiv \theta_{12}$ the angle formed by the bound electron position vectors $\vec{r}_1$ and $\vec{r}_2$. After a lengthy algebra, proper account of the orthonormality and the $\langle\psi_{2s^2}|H|\psi_{2p^2}\rangle$ interaction, and then graphical optimization of $\gamma$ and $\delta$, we obtained: $\gamma=1.9245$, $\delta=1.7715$; $C=5.1368$, $c=1.974\,77$, and $D=4.8231$. With these parameters, the mixing coefficients take values $c_{2s^2}=0.846\,64$, $c_{2p^2}=0.532\,16$, closely approaching the values $\frac{\sqrt{3}}{2}$ and $\frac{1}{2}$ long ago predicted by Rau in his $Z$-independent group theoretical approach [50]. The strong admixture with the virtual $2p^2$ state is the most striking manifestation of the insufficience of the single configuration description. The presentation in detail of the analytical procedure and of its generalization are out of the scope of this paper.

Within the two-configuration description of Eq. (15), the energy amounts to $E=-3.5414$ a.u., which is a value lying remarkably close to the $E=-3.542$ a.u. of the Jastrow function, and by far improves the poor response of the HF calculation, $E=-3.477$ a.u. It is perhaps worth noticing that, although $\psi$ does not rigorously satisfy any of the three $r_1$, $r_2$, $r_{12}$ cusp conditions, it nearly satisfies the former two conditions since $c+\gamma=3.899\approx Z$.

For the $1s^2$ ground state, we used the simple one-configuration form

$$\psi_{1s^2} = \frac{1}{4\pi} R_{1,0}(r_1) R_{1,0}(r_2), \tag{19}$$

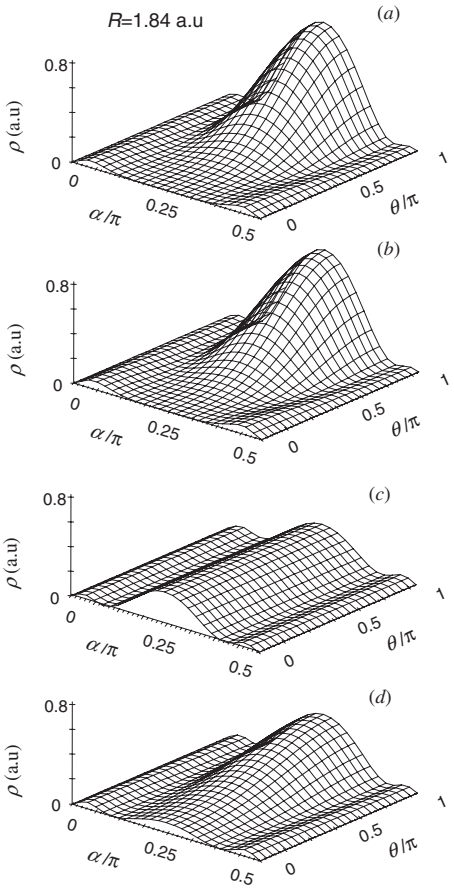


FIG. 1. Probability density $\rho$ (in a.u.) of the excited $Be^{2+}$ state $\psi$ [51], as a function of the hyperspherical coordinates $\alpha$ and $\theta$, on a dimensionless scale, $\alpha/\pi$ and $\theta/\pi$, respectively, and for hyperradius kept fixed at the value $R=\langle R\rangle=1.84$ bohrs. (a) Jastrow wave function [Eq. (13)]; (b) wave function from analytic global optimization [Eqs. (15)–(18)]; (c) same as (b) but after suppression of $\psi_{2p^2}$ and optimization of the $\psi_{2s^2}$ component alone; (d) "HF" wave function.

$$R_{1,0} = Be^{-\beta r}, \tag{20}$$

with $B=14.162\,11$, $\beta=3.6875$. As expected, its energy, $-13.598$ a.u., is above the prediction of Eq. (14).

Figure 1 illustrates the probability density $\rho(\alpha,\theta) = 8\pi^2 R^4 (\sin^2\alpha)(\cos^2\alpha)|\psi|^2$ of the $2s^2$ state in hyperspherical coordinates, as a function of pseudoangle $\alpha=\arctan\frac{r_2}{r_1}$ and angle $\theta$, for a hyper-radius $R=\sqrt{r_1^2+r_2^2}$ kept fixed at the mean value $R=1.84$ a.u. [51]. The localization of the probability around the ridge $\alpha=\frac{\pi}{4}$ and $\theta=\pi$ is particularly pronounced in the case of the two fully correlated functions of Eqs. (13) and (15). Interestingly, these two functions, despite their different construction, show indistinguishable density plots [Figs. 1(a) and 1(b), respectively]. The quality of the function is proportional to the degree of localization of the probability along the Wannier ridge, representing a highly correlated electron pair at classical positions $\vec{r}_1\approx-\vec{r}_2$. Note that, upon optimization of the $2s^2$ configuration alone, a distorted density distribution is obtained [Fig. 1(c)] in which the angular correlation is no longer present, but in which part of the radial correla-

tion still is present [52]. Finally, significant flattening of the distribution is observed upon using the poorly correlated HF function [Fig. 1(d)].

## III. RESULTS AND DISCUSSION

In order to probe electron-electron correlation, analyze the ionization mechanisms, and determine the most favorable working conditions for potential future experiments, we now proceed by studying how the fivefold fully differential cross section varies as a function of the energy values of the incident and the two ejected electrons, $E_i$, $E_1$, and $E_2$, respectively, and as a function of the directions of the three emerging electrons with respect to that of the incident one. These directions are given by the polar angles $\theta_s$, $\theta_1$, and $\theta_2$ for the scattered and the two ejected electrons, respectively, and vary from 0° to 360° in coplanar geometry ($\phi_s=\phi_1=\phi_2=0$).

### A. Variation of FDCS with $E_i$ and $\theta_s$

#### 1. $\theta_1=50°$, $\theta_2=270°$, $E_1=E_2$

Among all possible scenarios, we first consider that the two ejected electrons have the same energy $E_1=E_2=10$ eV and that their ejection angles are $\theta_1=50°$ and $\theta_2=270°$, which are directions of favorable ejection (see below). Figures 2(a) and 2(b) show the variations of the FDCS, in the latter geometry, as a function of the energy of the incident electron. Figures 2(a) and 2(b) refer to ionization of the outer shell ($L$) and inner shell ($K$), respectively. Here, all we need is that the scattering angles be small in order for the process to be effective. Their values are fixed arbitrarily at $\theta_s=0.2°$ ($L$-shell ionization) and 0.1° ($K$-shell ionization). As expected, the ionization of the $L$ shell is overall far more likely to occur than is the ionization of the $K$ shell, since the core electrons are much more tightly bound to the atom than are the valence electrons. Figure 2(a) ($L$-shell ionization) shows a distinct maximum at $E_i=5$ keV, whereas Fig. 2(b) ($K$-shell ionization) displays the maximum at $E_i=80$ keV. Physically, a nearly undeviated trajectory for the scattered electron is the signature of a non-head-on collision between the projectile and the atomic target, during which the incident electron interacts with the cloud of the atomic electrons rather than with the nucleus itself. This is to be contrasted with events in which the scattered electrons are strongly deviated, revealing a mechanism of frontal collisions between projectile and nucleus. It is the first of these mechanisms that is relevant here, showing that the double ionization essentially proceeds through electron-electron interactions [Figs. 2(a) and 2(b)]. In contrast to this mechanism, which is much more effective in the kinematics at hand, the other mechanism results in a reduced number of ionization events, as the fast projectile only weakly perturbs the bound electrons, and especially the valence ones which are farther away from the Be nucleus.

#### 2. $\hat{k}_1=\hat{K}$, $\hat{k}_1\perp\hat{k}_2$, $E_1=E_2$

Let us now turn our attention to another kinematical situation with $E_1=E_2$, in which the momentum vectors of the ejected electrons are orthogonal to each other and one of those is parallel to the momentum transfer $\vec{K}$. This orientation has some advantages and displays some interesting potentially observable structure, in particular upon considering the variation of the FDCS with the scattering angle. Figures 3(a) and 3(b) refer to this kinematics, with parameters fixed at $E_1=E_2=15$ eV, and for $E_i=5$ ($L$-shell ionization) and 20 keV ($K$-shell ionization), respectively. In both cases, a maximum is observed, which is located at $\theta_s=2.6°$ ($L$-shell ionization) and 1.1° ($K$-shell ionization). It turns out that these peaks correspond to those events for which the momentum transfer $\vec{K}=\vec{k}_i-\vec{k}_s$ and the momentum $\vec{k}_1$ of the electron that is ejected parallel to $\vec{K}$ happen to have nearly equal magnitudes. According to the equation for conservation of momentum, the recoil $\vec{q}$ of the residual ion becomes almost equal (in magnitude) and opposite (in direction) to the momentum $\vec{k}_2$ of the second ejected electron. Such a geometry, in which ion and electron emerge in nearly opposite directions, is classically optimal, and a little algebra allows us to verify this prediction. Thus, on account of the equations for conservation of energy, $E_i=E_s+2E_1+I_{2+}+\frac{\vec{q}^2}{2M}$, and momentum, $\vec{K}=\vec{k}_1+\vec{k}_2+\vec{q}$, a simple expression for the scattering angle is obtained for this geometry:

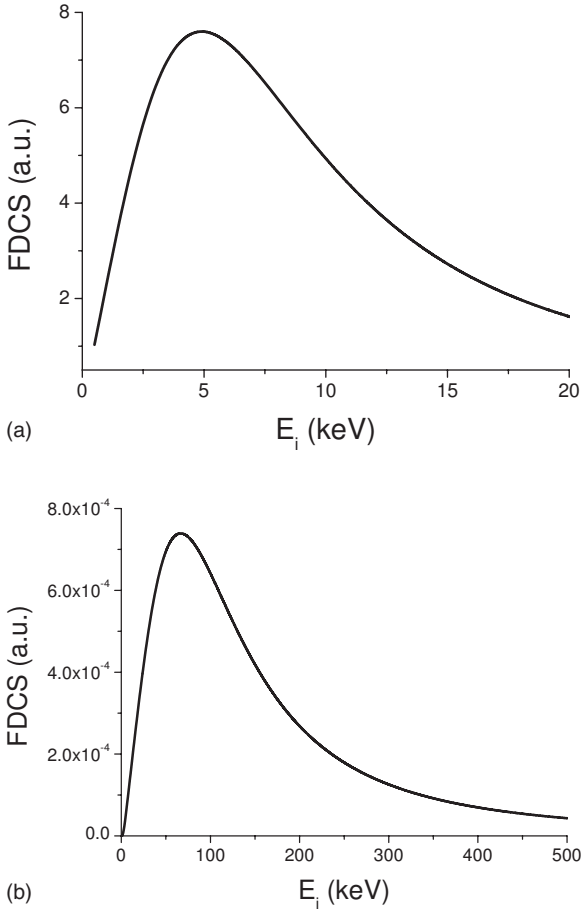


FIG. 2. FDCS (in a.u.) as a function of $E_i$ (in keV), and for a fixed scattering angle $\theta_s$, in the kinematics $\theta_1=50°$, $\theta_2=270°$, $E_1=E_2=10$ eV. (a) $L$-shell ionization, $\theta_s=0.2°$; (b) $K$-shell ionization, $\theta_s=0.1°$. The Jastrow wave functions were used for both the initial and the final states.

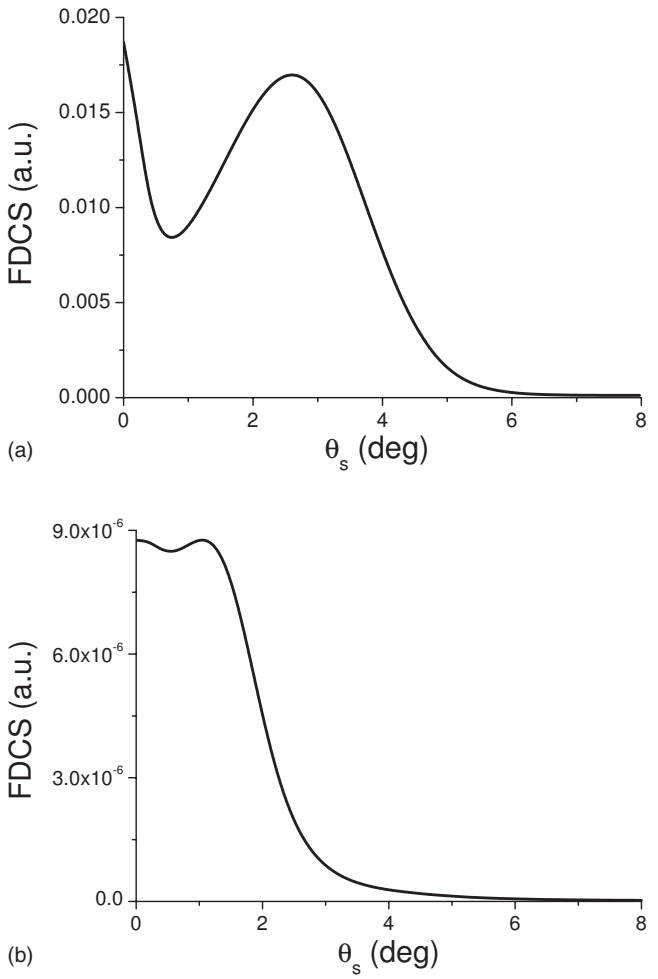


FIG. 3. FDCS (in a.u.) as a function of the scattering angle $\theta_s$ (in degrees), and for a fixed incident energy $E_i$, in the kinematics $\hat{k}_1 = \hat{K}$, $\hat{k}_1 \perp \hat{k}_2$, $E_1 = E_2 = 15$ eV. (a) *L*-shell ionization, $E_i = 5$ keV; (b) *K*-shell ionization, $E_i = 20$ keV. The Jastrow wave functions were used for both the initial and the final states.

$$\cos\,\theta_s \approx \left(E_i - \frac{3}{2}E_1 - \frac{I_{2+}}{2}\right) E_i^{-1/2}(E_i - 2E_1 - I_{2+})^{-1/2}, \tag{21}$$

where $M$ is the mass of the Be atom, and $I_{2+}$ is the double ionization energy, which takes the values $I_{2+} = 1.011\,65$ a.u. (*L*-shell ionization) and $I_{2+} = 11.171\,89$ a.u. (*K*-shell ionization). This expression predicts $\theta_s = 3.1°$ (*L*-shell ionization) and 1.5° (*K*-shell ionization), which are values differing by only about 0.5° from the quantum-mechanical results.

### B. Variation of FDCS with $E_1$ and $E_2$: Back to $\theta_1 = 50°$, $\theta_2 = 270°$

In order to give guidance to the experimentalist, which is one of the principal aims of the paper, here we confine ourselves to the geometry $\theta_1 = 50°$ and $\theta_2 = 270°$, which is particularly favorable in terms of yield. Both the projectile energy and the scattering angle are kept fixed at $E_i = 5$ keV, $\theta_s = 0.2°$ (*L*-shell ionization) and $E_i = 20$ keV, $\theta_s = 0.1°$ (*K*-shell ionization). No constraint $E_1 = E_2$ is imposed any longer, hence allowing us to understand how variations of $E_1$ and $E_2$ affect the FDCS.

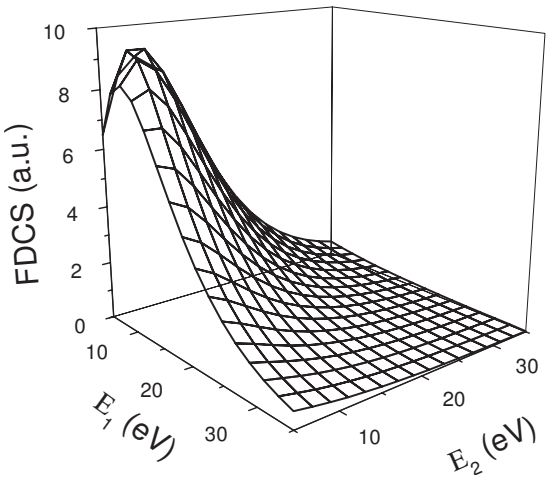


FIG. 4. FDCS (in a.u.) for *L*-shell double ionization, as a function of ejection energies $E_1$ and $E_2$ (in eV), in the kinematics $\theta_1 = 50°$, $\theta_2 = 270°$. The energy of the projectile is fixed at $E_i = 5$ keV and the scattering angle is $\theta_s = 0.2°$. The Jastrow wave functions were used for both the initial and the final states.

Figure 4 shows the variation of the FDCS, for *L*-shell ionization, in terms of the corresponding ejection energy values. For clarity, the origin of the two horizontal axes in this illustration has been taken at 5 eV. Only values below 35 eV for the energy of the ejected electrons produce appreciable amounts of yield. The maximum is produced at $E_1 = 7$ eV, $E_2 = 9$ eV, and the distribution is virtually symmetrical upon the exchange $E_1 \rightleftarrows E_2$. While in the case (not developed in this paper) of electrons ejected in opposite directions the energy is distributed nonuniformly between the two electrons [53], in the present case the near symmetry $\sigma^{(5)}(E_1,E_2) \approx \sigma^{(5)}(E_2,E_1)$ is an expected result. It is readily verifiable that, here, the ejection directions are nearly symmetrical with respect to the direction of the momentum transfer vector $\vec{K}$, which is a symmetry axis. The bisecting line between the ejection directions forms an angle of 340° with the incidence direction ($z$ axis), which is a value differing by only 8° from the $\vec{K}$ axis ($\theta_K \approx 348°$).

The variation of the FDCS for *K*-shell ionization is depicted in Fig. 5. Qualitatively similar trends to those displayed on Fig. 4 are observed. On quantitative grounds, the cross sections for *K*-shell ionization are overall far smaller than the ones for *L*-shell ionization. This is one of the common characteristics of the ionization of inner shells, the electrons of which are bound tightly to their atoms. As before, here again the direction of $\vec{K}$ ($\theta_K \approx 354°$) lies close to the bisecting line between the ejection directions, which results in nearly symmetrical cross sections.

### C. Variation of FDCS with $\theta_1$ and $\theta_2$: $E_1 = E_2$

How the FDCS varies in terms of the ejection angles $\theta_1$ and $\theta_2$ is one of the most interesting tasks of this study, and

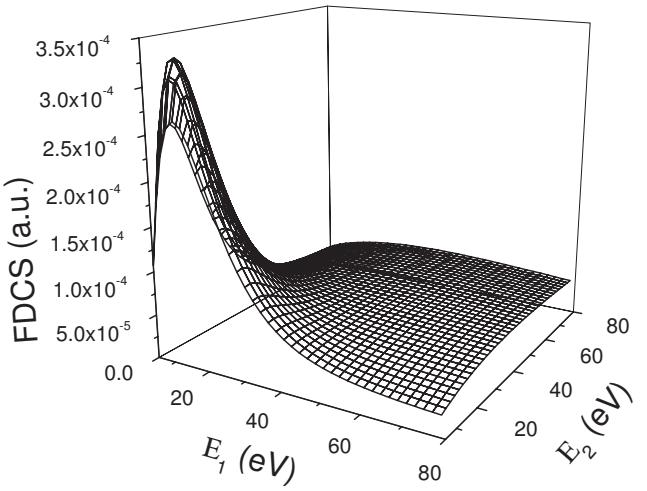


FIG. 5. Same as in Fig. 4 but for $K$-shell ionization, with $E_i=20$ keV and $\theta_s=0.1°$.

may serve as a sensitive probe of electron correlation. Equal ejection energy values are assumed, but no constraint is imposed as to the relative geometry of $\hat{k}_1$ and $\hat{k}_2$. The fully correlated Jastrow wave functions are used for both the Be ground state and the two $Be^{2+}$ states. Figure 6 shows the contour plot of the FDCS for $L$-shell ionization, with $E_1=E_2=10$ eV, and $E_i$ and $\theta_s$ kept fixed at 1.5 keV and 0.2°, respectively. The areas of large cross sections are indicated by darker shades of gray. A well-defined "four-island" symmetric structure is obtained. This pattern is a consequence of the remnants of the dipole selection rules, still quite prominent at small momentum transfer. Note parenthetically that, although the He 1$s$ orbital has no node, a similar topological structure also characterizes its FDCS [54]. As shown below, this is also the case with the Be $K$-shell ionization, which involves orbitals with different nodal structure. These observations show clearly that such a characteristic pattern by no means should be interpreted as manifestation of the nodal structure of electron orbitals. It is worth pointing out that, in helium, for a modest momentum transfer $K<1$, the topological structures of the $(e,3e)$ and $(\gamma,2e)$ FDCSs are very similar [54]. We can thus reasonably expect this to be also the case in Be.

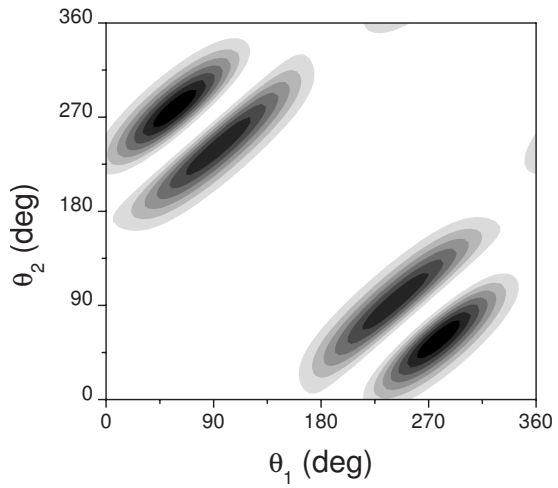


FIG. 6. Gray-scale representation of the FDCS (in a.u.), for $L$-shell double ionization, as a function of the ejection angles $\theta_1$ and $\theta_2$ and for equal asymptotic energies $E_1=E_2=10$ eV. The energy of the projectile is fixed at $E_i=1.5$ keV and the scattering angle is $\theta_s=0.2°$. The Jastrow wave functions were used for both the initial and the final states. $\vec{K}$ in polar coordinates is (0.172 a.u., 347.9°).

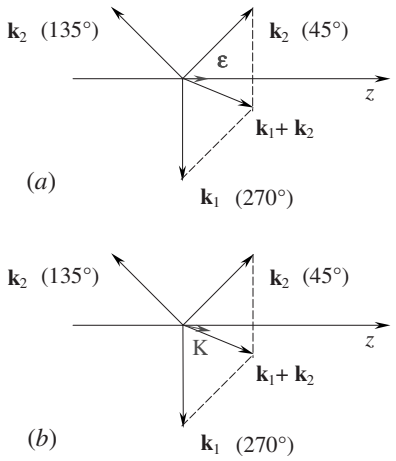


FIG. 7. Schematic representation of the wave vectors of the ejected electrons for the geometries ($\theta_1=270°$, $\theta_2=45°$) and ($\theta_1=270°$, $\theta_2=135°$). (a) $(\gamma,2e)$ with $\vec{\varepsilon}$ the photon polarization vector; (b) $(e,3e)$ with $\vec{K}$ the momentum transfer.

The outer island of Fig. 6, aligned with the $\vec{K}$ direction, is identified as the "binary peak." The inner one, aligned with $-\vec{K}$, is the "recoil peak." The area of vanishing cross section around the principal diagonal $\theta_1 \approx \theta_2$ results from Coulomb repulsion, whereas the regions of virtually vanishing cross section, separating the recoil peak from the binary peak, result, as noted above, from the remnants of the dipole selection rules. Despite the striking similarity in the overall structure of the contour plots between beryllium $(e,3e)$ $L$-shell ionization (Fig. 6) and helium $(e,3e)$ [54], our FDCSs show considerably narrower angular widths of the correlation pattern than do their helium counterparts. This width is known to control how closely the electrons can approach each, other favoring the back-to-back emission. This observation suggests a much stronger angular correlation in Be as compared to He. This is in agreement with the argument that the strength of the angular correlation in the two-electron continuum is proportional to the time spent by the ejected electrons in the Wannier trajectory [55]. Given the large electron radius of Be, one expects a larger spatial extent of the Coulomb zone, and thus stronger angular correlations.

At this stage, a brief comparative analysis between $(e,3e)$ and $(\gamma,2e)$ deserves some attention. With this purpose, we focus momentarily on the specific ejection geometries ($\theta_1=270°$, $\theta_2=45°$) and ($\theta_1=270°$, $\theta_2=135°$). According to Fig. 6, these directions lie in the deep interior of the two peaks and are highly favorable. They are moreover symmetric to each other with respect to the direction ($\theta_1=270°$, $\theta_2=90°$), which is strictly forbidden at $E_1=E_2$. They are illustrated schematically in Fig. 7. In $(\gamma,2e)$, they both result in equal amounts of yield [Fig. 7(a)], which is a result issuing from

the equivalence between the directions $\hat{\varepsilon}$ and $-\hat{\varepsilon}$ along the polarization axis of light (the $z$ axis on Fig. 7). Rather, in $(e,3e)$ [Fig. 7(b)], it is the former geometry ($\theta_1=270°$, $\theta_2=45°$) that is more favorable, resulting in an ion recoil $\vec{q}=\vec{K}-\vec{k}_1+\vec{k}_2$ that is small and practically parallel to the momentum transfer. This is quite a general property: the difference between $(e,3e)$ and $(\gamma,2e)$ is in the relative intensity of the two islands in each group. In $(\gamma,2e)$, the direction along $\hat{\varepsilon}$ is equivalent to the direction opposite to it. In $(e,3e)$, due to a final momentum transfer, the directions $\vec{K}$ and $-\vec{K}$ are not equivalent any longer. Thus, one of the islands acquires more intensity relative to its counterpart. In Fig. 6, it is the outer island, aligned with the $\vec{K}$ direction, which is more prominent. In He $(e,3e)$, this feature is consistent with the experiment [56] and with sophisticated CCC calculations [54], but disagrees with previous 3C predictions [54] placing more intensity on the recoil peak as compared to a weaker binary peak. It was later shown that the latter inconsistency was actually an artifact, which could be corrected by a proper account of the dynamical screening of the nuclear charge by one of the outgoing electrons [57]. When the screening effect is properly accounted for, it is the outer island of intensity, aligned with the $\vec{K}$ direction, that becomes more prominent. The fact that our 3C calculation produces the correct pattern adds credibility to our treatment of the Be problem, and can be a stringent criterion for reliability.

In order to assess what the effects of the initial state electron correlation are on the double ionization cross sections, we also did FDCS calculations with Jastrow's less correlated variant and the Clementi function, and compared with the FDCS of Fig. 6. In all three cases, practically indistinguishable contour plots were obtained (not shown). To make the comparison conclusive, Fig. 8 illustrates how the FDCS varies along the straight line intersecting the islands from the top left to the bottom right, $\theta_1+\theta_2=2\theta_K-360°$, where $\theta_K$ is the obtuse angle between the $\vec{K}$ direction and the $z$ axis. The degree of the electron correlation of the initial state was found to have some effect on the extents of both the central area and the valley between binary and recoil peaks. On passing from the Clementi wave function, which contains only a poor amount of correlation, to the fully correlated Jastrow function, the central area is shown to shrink by about 6°, whereas the region separating the recoil peak from the binary peak broadens by almost the same amount. For all three initial state wave functions, we found equal angular widths for the binary peak, and a steadily increasing width, from 19° to 22°, for the recoil peak. As regards magnitudes, the electron correlation affects significantly the height of both peaks, which is decreased with increasing degree of correlation.

For *K*-shell ionization, the incident electron energy was fixed at 11 keV and the scattering angle at $\theta_s=0.1°$. Figure 9 shows contour plots that are qualitatively similar to the ones for *L*-shell ionization, exhibiting as before a well-pronounced four-island symmetric structure. Again, our 3C calculation places more intensity on the binary peak than in the recoil peak, in agreement with state-of-the-art CCC and 3C calculations and experiments on helium. As in the *L*-shell ionization case, the unbalanced amount of intensity shared

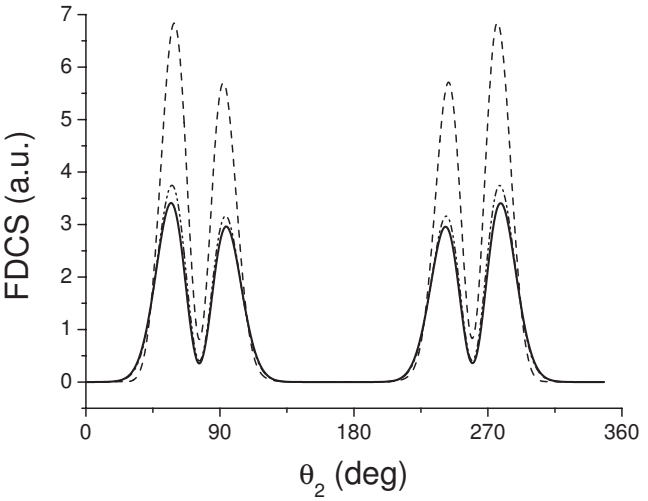


FIG. 8. Variation of the FDCS (in a.u.) for *L*-shell double ionization, as a function of the ejection angle $\theta_2$ in the direction defined by $\theta_1+\theta_2=2\theta_K-360°$, for the same energy values as in Fig. 6. All the calculations were done with the Jastrow fully correlated function for the ion state. For the Be state: Jastrow's fully correlated function (solid line); the less correlated Jastrow variant (dash-dotted curve); Clementi function (dashed curve). $\vec{K}$ in polar coordinates is (0.172 a.u., 347.9°).

by the two peaks stems from the natural asymmetry between the $\pm\hat{K}$ directions, which in $(e,3e)$ are no longer equivalent. Interestingly enough, the contrast between the amounts of intensity placed on each of the two peaks is much more marked here than it was for *L*-shell ionization. This is a consequence of *K*'s characteristic property to increase (for a scattering angle kept fixed) in the same proportion as the values of the incident and scattered electron energy, hence further enhancing the asymmetry between the two opposite $\pm\hat{K}$ directions. The same conclusions as those for the *L*-shell ionization case are also drawn about the way in which the electron correlation in the initial state affects the extent of the

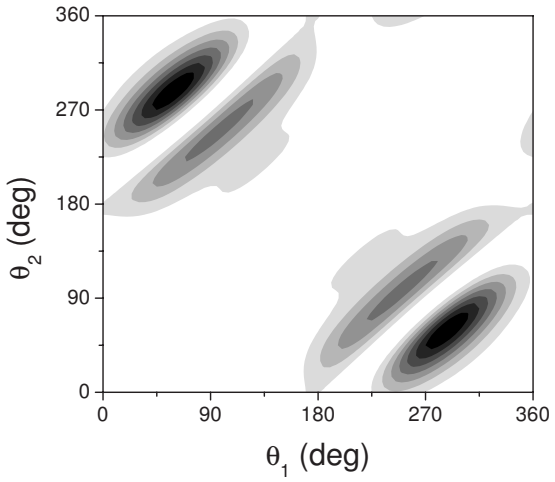


FIG. 9. Same as in Fig. 6, but for *K*-shell ionization, with $E_i=11$ keV and $\theta_s=0.1°$. $\vec{K}$ in polar coordinates is (0.425 a.u., 353.4°).

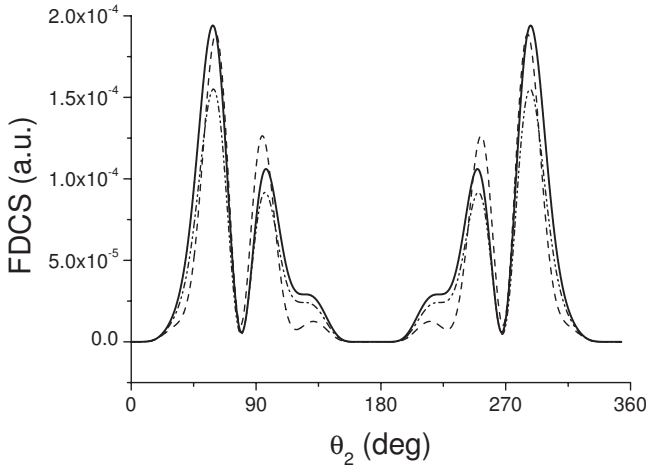


FIG. 10. Variation of the FDCS (in a.u.) for $K$-shell double ionization, as a function of the ejection angle $\theta_2$ in the direction defined by $\theta_1+\theta_2=2\theta_K-360°$, for the same energy values as in Fig. 9. All the calculations were done with the Jastrow fully correlated function for the ion state. For the Be state: Jastrow's fully correlated function (solid line); the less correlated Jastrow variant (dash-dotted curve); Clementi function (dashed curve). $\vec{K}$ in polar coordinates is (0.425 a.u., 353.4°).

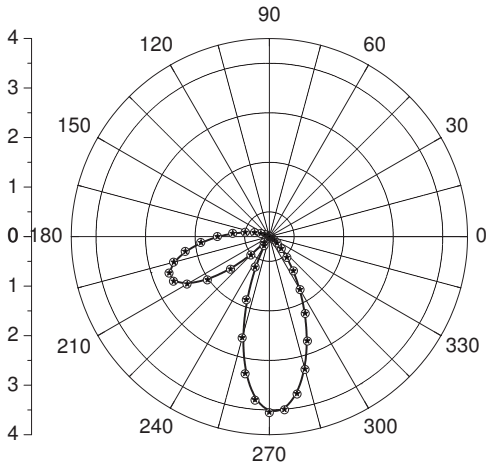


FIG. 11. Polar representation of the FDCS (in a.u.) for $L$-shell double ionization, for equal asymptotic ejection energies $E_1=E_2=10$ eV, as a function of the ejection angle $\theta_2$, with $\theta_1=50°$. The energy of the projectile is fixed at $E_i=1.5$ keV and the scattering angle is $\theta_s=0.2°$. All the calculations were done with the Jastrow fully correlated function for the Be initial state. For the ion state: Jastrow's fully correlated function (solid line); analytic global optimization (filled stars); Hartree-Fock (empty circles).

central zone and of the adjoint straps. According to Fig. 10, the $K$-shell ionization affects the angular widths of the shapes more significantly than does the $L$-shell ionization, showing both the binary peak and the recoil peak to broaden on passing from the Clementi wave function to the fully correlated Jastrow function. This trend, which is opposite to an expected narrowing upon gradual increase of the electron correlation in the ground state, should shed more light on the controversy [31,58] as to the origin of the effect, and the possible role of the Compton profile of the target orbital. While in the ionization case at hand the effects of improvement in electron correlation on the height of the peaks are less pronounced than before, now these effects produce both negative and positive contributions. Clearly, this is the imprint of some delicate interplay between two heavily mixed $f_1$ and $f_2$ integrals. The latter finding once more underlines the need for a global treatment of all four electrons as "performers."

The characteristic of the double ionization problem in beryllium, as compared to that in helium, is that we are left with a two-electron ion. In past treatments, the influence of the inner electrons has been effectively considered with model or polarization potentials for core effects. In the present paper, all the electrons participate actively in the FDCS. In order to assess the relative effects of the residual ion electrons on the ionization FDCS, final state wave functions with varying degree of correlation are now checked for the same initial state wave function. Figures 11 and 12 show polar plots of the variation of the FDCS, for $L$-shell ionization and for $K$-shell ionization, respectively. In these plots, the polar radius represents the magnitude of the FDCS and the polar angle is $\theta_2$. The ejection angle $\theta_1$ is kept fixed at 50° and the ejection energies are $E_1=E_2=10$ eV. The incident energy values are $E_i=1.5$ ($L$-shell ionization) and 11 keV ($K$-shell ionization). In the case of the $L$-shell ionization (Fig. 11), any variations in the electron correlation of the $1s^2$ $Be^{2+}$ state are of virtually no effect on the pronounced two-lobe FDCS structure. At the end of the process, we are left with an effective "helium bare nucleus" target.

This is not the case with the ionization of the $K$ shell, in which the effects of improvement in electron correlation on the shape and magnitude of the two lobes are substantial. Thus, increase of the degree of correlation in the ion state wave function results in striking enhancement of the FDCS, along with significant increase of the recoil lobe (known to favor the backward ejection of one of the electrons) relative to its dominant counterpart. This is a consequence of now strongly interfering exchange integrals $f_1$ and $f_2$, and of electron orbital overlaps that are particularly sensitive to the variations of the electron correlation in the ion state. Remarkably, the two wave functions of Figs. 1(a) and 1(b), whose plots look virtually identical, turn out to produce pro-

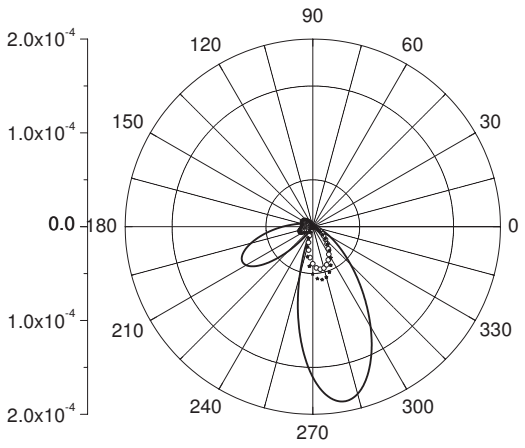


FIG. 12. Same as in Fig. 11, but for $K$-shell ionization, with $E_i=11$ keV and $\theta_s=0.1°$.

nounced changes both in the magnitude and in the shape of the FDCS. This observation once more underlines the need for a rigorous all-electron treatment and for highly correlated functions.

In view of the different trends observed in the two cases of ionization as a function of the quality of the final state input wave functions, working experimentally, in the conditions described above, with both *K*-shell and *L*-shell channels, and then establishing FDCS($LL$) to FDCS($KK$) ratios (which are measurable quantities free of calibration factors), can be particularly effective in quantifying electron-electron correlation.

## IV. SYNOPSIS

The primary aim of this work was to predict and probe measurable quantities in the $(e,3e)$ process with as target neutral atomic beryllium. To this purpose, we carried out calculations of fully differential cross sections for double ionization of the *L* and *K* atomic shells. The 3C method was employed to represent the correlated wave function in the double continuum of the ejected electrons. In order to assess the relative effects of electron-electron interactions, compact Jastrow and other analytical wave functions were developed for the bound or quasibound initial or final states of the target. Favorable suitable conditions were determined, in terms of geometry, incident electron energy, scattering angle, ejection energy, and angles of ejection, in order for the yield to be optimal and the process technically feasible. The $(e,3e)$ process was found, as to some trends, to have much in common with $(\gamma,2e)$, allowing to some extent for parallels between double ionization by fast electron impact and photo-double-ionization. It was shown that quantum-mechanical simulations, when sufficiently accurate to realistically model the complex electronic interactions of bound, quasibound, or continuum states, can provide concrete predictions to guide future $(e,3e)$ experiments. $(e,3e)$ experiments, which at the current state of the art solely address low-complexity atomic targets, bring much insight into the study of hollow atoms and ions, whose states are known to contain a huge amount of electronic correlation. We believe that our results will be an important support for ongoing experimental investigations in beryllium using existing setups for coincidence experiments.


[1] F. W. Byron, Jr. and C. J. Joachain, Phys. Rev. **164**, 1 (1967).
[2] R. J. Tweed, J. Phys. B **6**, 398 (1973).
[3] R. J. Tweed, Z. Phys. D **23**, 309 (1992).
[4] V. G. Neudatchin, Yu. F. Smirnov, A. V. Pavlitchenkov, and V. G. Levin, Phys. Lett. **64A**, 31 (1977).
[5] Yu. F. Smirnov, A. V. Pavlitchenkov, V. G. Levin, and V. G. Neudatchin, J. Phys. B **11**, 3587 (1978).
[6] C. Dal Cappello and H. Le Rouzo, Phys. Rev. A **43**, 1395 (1991).
[7] B. Joulakian, C. Dal Cappello, and M. J. Brauner, J. Phys. B **25**, 2863 (1992).
[8] B. Joulakian and C. Dal Cappello, Phys. Rev. A **47**, 3788 (1993).
[9] A. Lahmam-Bennani, C. Dupré, and A. Duguet, Phys. Rev. Lett. **63**, 1582 (1989).
[10] A. Lahman-Bennani, A. Duguet, A. M. Grisogono, and M. Lecas, J. Phys. B **25**, 2873 (1992).
[11] M. J. Ford, J. B. Doring, J. H. Moore, and M. A. Coplan, Rev. Sci. Instrum. **66**, 3137 (1995).
[12] A. Dorn, A. S. Kheifets, C. D. Schröter, B. Najjari, C. Höhr, R. Moshammer, and J. Ullrich, Phys. Rev. A **65**, 032709 (2002).
[13] P. Bolognesi, C. C. Jia, L. Avaldi, A. Lahmam-Bennani, K. A. Kouzakov, and Y. V. Popov, Phys. Rev. A **67**, 034701 (2003).
[14] R. W. van Boeyen, N. Watanabe, J. P. Doering, J. H. Moore, and M. A. Coplan, Phys. Rev. Lett. **92**, 223202 (2004).
[15] M. Takahashi, N. Watanabe, Y. Khajuria, K. Nakayama, Y. Udagawa, and J. H. D. Eland, J. Electron Spectrosc. Relat. Phenom. **141**, 83 (2004).
[16] C. Bouri, P. Selles, L. Malegat, and M. G. Kwato Njock, Phys. Rev. A **73**, 022724 (2006).
[17] M. Fiori, A. B. Rocha, C. E. Bielschowsky, G. Jalbert, and C. R. Garibotti, J. Phys. B **39**, 1751 (2006).
[18] S. Jones, D. H. Madison, and J. H. Macek, Nucl. Instrum. Methods Phys. Res. B **241**, 73 (2005).
[19] A. S. Kheifets and I. Bray, Phys. Rev. A **69**, 050701(R) (2004).
[20] A. S. Kheifets, Phys. Rev. A **69**, 032712 (2004).
[21] O. Chuluunbaatar, I. V. Puzynin, P. S. Vinitsky, Y. V. Popov, K. A. Kouzakov, and C. Dal Cappello, Phys. Rev. A **74**, 014703 (2006).
[22] S. Elazzouzi, C. Dal Cappello, A. Lahmam-Bennani, and F. Catoire, J. Phys. B **38**, 1391 (2005).
[23] R. Dey, A. C. Roy, and C. Dal Cappello, J. Phys. B **39**, 955 (2006).
[24] M. S. Pindzola, F. Robicheaux, and J. Colgan, J. Phys. B **39**, L127 (2006).
[25] R. P. Doerner, M. Baldwin, J. Hanna, Ch. Linsmeier, D. Nishijima, R. Pugno, J. Roth, K. Schmid, and A. Wiltner, Phys. Scr., T **128**, 115 (2007).
[26] F. Wang and B. Gou, J. Phys. B **36**, 331 (2003).
[27] M. Zhang, B. Gou, and L. Cui, J. Phys. B **38**, 3567 (2005).
[28] L. R. Wang, J. T. Hsiao, and K. N. Huang, J. Phys. B **39**, L217 (2006).
[29] S. Hasegawa, E. Recami, F. Yoshida, L. Matsuoka, F. Koike, S. Fritzsche, S. Obara, Y. Azuma, and T. Nagata, Phys. Rev. Lett. **97**, 023001 (2006).
[30] F. Yoshida, F. Koike, S. Obara, Y. Azuma, T. Nagata, and S. Hasegawa, Phys. Rev. A **75**, 012714 (2007).
[31] A. S. Kheifets and I. Bray, Phys. Rev. A **65**, 012710 (2001).
[32] A. S. Kheifets and I. Bray, J. Phys. B **36**, L211 (2003).
[33] J. Colgan, S. D. Loch, M. S. Pindzola, C. P. Ballance, and D. C. Griffin, Phys. Rev. A **68**, 032712 (2003).
[34] A. V. Nefiodov and G. Plunien, Phys. Lett. A **363**, 115 (2007).
[35] H. Bachau, P. Galan, and F. Martin, Phys. Rev. A **41**, 3534 (1990).
[36] For an analysis of the autoionization dynamics and the life-

times of high-lying doubly excited states in light or heavy two-electron ions; see, for instance, [37] and [38], respectively.
[37] M. Chrysos, Y. Komninos, Th. Mercouris, and C. A. Nicolaides, Phys. Rev. A **42**, 2634 (1990).
[38] B. C. Gou, Z. Chen, and C. D. Lin, Phys. Rev. A **43**, 3260 (1991).
[39] R. Jastrow, Phys. Rev. **98**, 1479 (1955).
[40] J. D. Talman, Phys. Rev. A **21**, 1805 (1980).
[41] N. Umezawa, A. Sarsa, C. Le Sech, and T. Chikyow, Phys. Rev. A **73**, 012512 (2006).
[42] C. Le Sech, J. Phys. B **30**, L47 (1997).
[43] D. Sundholm, J. Olsen, P.-A. Malmquist, and B. O. Roos, in *Numerical Determination of the Electronic Structure of Atoms, Diatomic and Polyatomic Molecules*, edited by M. Defranceschi and J. Delhalle (Kluwer, Dordrecht, 1989), p. 329.
[44] E. Lindroth, H. Persson, S. Salomonson, and A.-M. Martensson-Pendrill, Phys. Rev. A **45**, 1493 (1992).
[45] E. Clementi and C. Roetti, At. Data Nucl. Data Tables **14**, 177 (1974).
[46] M. Brauner, J. S. Briggs, and H. Klar, J. Phys. B **22**, 2265 (1989).
[47] For multiparameter problems, absolute minimum search procedures are not always guaranteed.
[48] G. Tanner, K. Richter, and J.-M. Rost, Rev. Mod. Phys. **72**, 497 (2000).
[49] G. W. F. Drake, Can. J. Phys. **66**, 586 (1988).
[50] A. R. P. Rau, Rep. Prog. Phys. **53**, 181 (1990).
[51] The definition of the density $\rho$ used in the text was made according to $\int_0^\infty \int_0^\infty \int_0^\pi \rho \, dr_1 dr_2 \sin\theta \, d\theta = 1$.
[52] Strictly, in higher levels of excitation, $n \gg 2$, the electron probability density of the lowest-lying $^1S$ state within a given $n$ manifold exhibits an even more complicated pattern, thereby revealing an interesting modal dynamics. To get an idea of what such plots look like for $n_1 = n_2 \gg 2$, see, for instance, Fig. 4(a) in [38].
[53] This $(e,3e)$ result, obtained for the geometry $\hat{k}_1 = -\hat{k}_2 = \hat{K}$, agrees with some $(\gamma,2e)$ results from an exemplified mathematical model for Be [34] [see also M. Ya Amusia, E. G. Drukarev, V. G. Gorshkov, and M. P. Kazachkov, J. Phys. B **8**, 1248 (1975)].
[54] A. S. Kheifets, I. Bray, J. Berakdar, and C. Dal Cappello, J. Phys. B **35**, L15 (2002).
[55] S. Cvejanović and T. Reddish, J. Phys. B **33**, 4691 (2000).
[56] A. Lahmam-Bennani, A. Duguet, M. N. Gaboriaud, I. Taouil, M. Lecas, A. Kheifets, J. Berakdar, and C. Dal Cappello, J. Phys. B **34**, 3073 (2001).
[57] J. R. Götz, M. Walter, and J. S. Briggs, J. Phys. B **39**, 4365 (2006).
[58] F. Citrini, L. Malegat, P. Selles, and A. K. Kazansky, Phys. Rev. A **67**, 042709 (2003).